

# Topology optimization for considering distortion in additive manufacturing

Takao Miki<sup>a,\*</sup>, Takayuki Yamada<sup>b</sup>

<sup>a</sup>*Osaka Research Institute of Industrial Science and Technology, 7-1, Ayumino-2, Izumi-city, Osaka, 594-1157, Japan*

<sup>b</sup>*Department of Strategic Studies, Institute of Engineering Innovation, The University of Tokyo, 11-16, Yayoi-2, Bunkyo-ku, Tokyo, 113-8656, Japan*

---

## Abstract

This paper proposes a topology optimization method that takes account of distortion induced by additive manufacturing (AM). AM is a free-form manufacturing technique in which the part is built in a layer-by-layer manner. In particular, laser powder bed fusion (LPBF) is one of the most widespread technologies for metal parts. However, LPBF is known to cause residual stress and distortion during fabrication, which adversely affects the mechanical properties and dimensional accuracy of the part. Therefore, predicting and avoiding the residual stress and distortion are critical issues. Our goal is to propose a topology optimization method that considers distortion in AM and an analytical model of AM suitable for incorporation into topology optimization. First, we propose an analytical model of the AM building process by LPBF, and formulate an optimization problem. Next, a topological derivative of the objective functional is approximately derived using an adjoint variable method and is utilized to update the level set function via a time evolutionary reaction-diffusion equation. Finally, two-dimensional design examples demonstrate the validations and effectiveness of the proposed optimization methodology.

*Keywords:* Topology optimization, Level set method, Metal additive manufacturing, Inherent strain method

---

\*Corresponding author

*Email address:* mikit@tri-osaka.jp (Takao Miki)

## 1. Introduction

Topology optimization [1, 2] has been widely used in industry for designing high-performance structures, but these structures are often complicated shape and cannot be manufactured directly by conventional technologies such as machining and molding. To solve this problem, manufacturability needs to be considered in the optimization procedure. For instance, topology optimization methods such as controlling the length scale [3, 4] or avoiding internal voids and undercut shapes in molding [5, 6, 7] have been proposed to ensure the optimal shape which is manufacturable. On the other hand, metal additive manufacturing (AM) is attracting attention as a free-form manufacturing technique that can build complicated shapes in a bottom-up, layer-by-layer manner. In particular, laser powder-bed fusion (LPBF) is utilized in various applications including aerospace, automotive, medical, energy, etc. However, in LPBF, manufacturability such as overhang constraint needs to be considered and several approaches have been proposed to incorporate it into topology optimization [8, 9, 10, 11, 12]. In addition, there remain things that must be considered to ensure that the fabrication does not fail, i.e. residual stress and distortion. Here, we focus on developing topology optimization that adds the reduction of part distortion induced by AM during the optimization procedure.

In the LPBF process, the material is melted and solidified by locally and rapidly heating and cooling. This process cycle generates inelastic strains such as thermal, plastic and transformation strains. These strains cause the residual stress and distortion, and adversely affect the strength and dimensional accuracy of the part. Therefore, predicting and avoiding the residual stress and distortion are crucial issues that make or break the product's success.

There are already many experimental and numerical works [13, 14, 15, 16, 17, 18, 19] on the residual stress and distortion. Methodologies based on numerical analysis can be sorted into two approaches: the thermal-elastic-plastic analysis method [20] and the inherent strain method [21, 22], originally used in the welding process. The thermal-elastic-plastic analysis method is a coupled analysis that combines heat transfer analysis and elastic or elastic-plastic analysis. In elastic-plastic analysis, it is necessary to consider the nonlinearity of the material properties and the solid-liquid phase transition. This analysis method using a detailed model that has a moving heat source and micro-scale layer thickness is computationally expensive. Because of

this, many simplified methodologies have been proposed in order to predict the residual stress and distortion on a part-scale [23, 24, 25, 26, 27, 28, 29]. However, it is difficult to replace the moving heat source with a simplified heat source, and few reports have validated the effectiveness of these analytical models. With the inherent strain method, the inherent strain component identified experimentally from the fabricated part is applied to an analysis domain, and the residual stress and distortion are obtained by linear elastic analysis. Therefore, it is computationally inexpensive compared to the thermal-elastic-plastic analysis method in that it does not need coupled analysis and nonlinear analysis. The effectiveness and validity of the method have already been reported by experimental verification [30, 31, 32]. Based on these numerical analysis methods, there have been a few proposed topology optimization methods that take into account reducing the residual stress or distortion of the AM part. Wildman et al. [33] proposed a multi-objective topology optimization method using the solid isotropic material with penalization scheme with the objective functional of the mean compliance and the reducing part distortion. A thermo-elastic element-birth model is proposed in which the elements are sequentially activated to simulate the moving heat source. Allaire et al. [34] proposed a layer by layer thermo-elastic analysis model and incorporated it into a level set-based topology optimization to minimize the distortion of each layer or the residual stress as an objective functional. In this approach, the optimal configuration obtained from a mean compliance minimization problem is reoptimized as the initial shape. By adding the mean compliance and a pre-defined stress threshold as constraints to the optimization problem, this optimization method succeeded in minimizing the sacrifice of mean compliance and reducing the residual stress. However, both approaches are computationally intensive due to the use of coupled analysis in the AM analytical model, which is not sufficient as an analytical model combined with topology optimization that requires the iterative procedure. In addition, the validity of the proposed analytical model has not been clarified.

In this study, this paper presents a topology optimization method that considers part distortion in AM, using a computationally inexpensive analytical model. Specifically, we propose an analytical model based on the inherent strain method that balances the accuracy of numerical analysis with computationally inexpensive cost to predict the residual stress and distortion, and incorporate the proposed model into the topology optimization procedure to obtain optimal configurations that provide high-performance considering the

part distortion in AM.

The remainder of this paper is organized as follows: In section 2, we propose an analytical model based on the inherent strain method for predicting the residual stress and distortion in the AM building process. Section 3 explains an identification method of the inherent strain component. Section 4 presents an experimental validation of the proposed analytical model. Section 5 explains the level set-based topology optimization method in which the level set function is updated using the reaction-diffusion equation. In Section 6, we formulate an optimization problem that incorporates the reduction of part distortion in the topology optimization procedure and derive an approximate topological derivative using variational analysis and the adjoint variable method. In Section 7, we then construct an optimization algorithm for the topology optimization using FEM. Section 8 presents two-dimensional design examples to demonstrate the validity of the proposed optimization methodology. Finally, Section 9 summarizes our study and provides conclusions. All numerical calculations were executed in FreeFEM++[35].

## 2. Analytical model for AM

In this section, the physics representing the layer-by-layer type building process in AM is modeled using the inherent strain method, a type of linear elastic analysis. The reason for using such a method is that optimization requires iterative calculations and therefore a model with computationally inexpensive cost is more suitable. To simplify the modeling, the present study assumes that a constant strain generates with each addition of the layer.

### 2.1. Inherent strain method

In the AM building process, inelastic strains such as thermal strain, plastic strain, and phase transformation strain are induced in the part through the material's melt-solidification cycle. The sum of these inelastic strains is called inherent strain [21, 22]. The total strain  $\boldsymbol{\varepsilon}(\mathbf{u})$  is defined by  $\boldsymbol{\varepsilon}(\mathbf{u}) := \frac{1}{2}(\nabla\mathbf{u} + (\nabla\mathbf{u})^\top)$  and can be divided into the elastic strain  $\boldsymbol{\varepsilon}^{el}$  and the inherent strain  $\boldsymbol{\varepsilon}^{inh}$ . That is, the inherent strain  $\boldsymbol{\varepsilon}^{inh}$  and the Cauchy stress tensor  $\boldsymbol{\sigma}$  are defined as

$$\boldsymbol{\varepsilon}(\mathbf{u}) = \boldsymbol{\varepsilon}^{el} + \boldsymbol{\varepsilon}^{inh}, \quad (1)$$

$$\boldsymbol{\sigma} = \mathbb{C}\boldsymbol{\varepsilon}^{el} = \mathbb{C}\boldsymbol{\varepsilon}(\mathbf{u}) - \mathbb{C}\boldsymbol{\varepsilon}^{inh}, \quad (2)$$

where  $\mathbb{C}$  is the fourth-order elasticity tensor. In the case of an isotropic elastic material, the above tensor is given by:

$$\mathbb{C}_{ijkl} = E \left( \frac{\nu}{(1+\nu)(1-2\nu)} \delta_{ij} \delta_{kl} + \frac{1}{2(1+\nu)} (\delta_{ik} \delta_{jl} + \delta_{il} \delta_{jk}) \right), \quad (3)$$

with Young's modulus  $E$ , the Poisson's ratio  $\nu$  and the Kronecker symbol  $\delta_{ij}$ . The residual stress and distortion can be predicted by linear analysis through the process of applying the inherent strain layer by layer. As shown

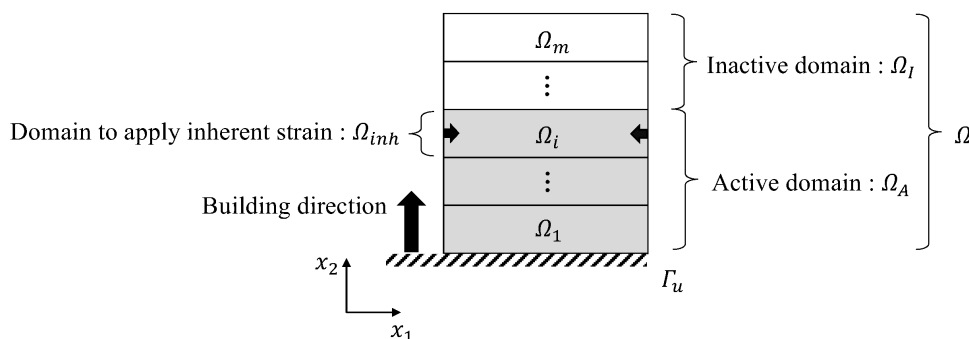


Figure 1: Domains and boundary in the middle of the building process.

in Fig. 1, let us consider an analysis domain  $\Omega$  that is divided into  $m$  layers with a fixed thickness in the building direction. The analysis domain  $\Omega$  is defined by each domain  $\Omega_i$  for  $1 \leq i \leq m$  as follows:

$$\Omega = \Omega_I \cup \dots \cup \Omega_i \cup \dots \cup \Omega_m. \quad (4)$$

Here we introduce three subdomains: active domain  $\Omega_A$ , inactive domain  $\Omega_I$ , and domain  $\Omega_{inh}$  to which inherent strain is applied. The subdomain region depends on the domain number  $i$ , and each subdomain is defined as

$$\Omega_A = \Omega_I \cup \dots \cup \Omega_i, \quad (5)$$

$$\Omega_I = \Omega \setminus \Omega_A, \quad (6)$$

$$\Omega_{inh} = \Omega_i \subset \Omega_A. \quad (7)$$

The active domain  $\Omega_A$  is filled with an elastic material and a fixed displacement boundary condition is applied to the bottom of the domain  $\Gamma_u$ . The

mechanical unknown of this model is the displacement field. The displacement  $\mathbf{u}_i \in \mathcal{U}$  with the inherent strain applied to the domain  $\Omega_{inh}$  is governed by the equations of linear elasticity, as follows:

$$\begin{cases} -\text{div}(\boldsymbol{\sigma}_i) = 0 & \text{in } \Omega_A, \\ \boldsymbol{\sigma}_i = \mathbb{C}\boldsymbol{\varepsilon}(\mathbf{u}_i) - \mathbb{C}\boldsymbol{\varepsilon}^{inh}, & \\ \mathbf{u}_i = \mathbf{0} & \text{on } \Gamma_u, \\ -\boldsymbol{\sigma}_i \cdot \mathbf{n} = \mathbf{0} & \text{on } \partial\Omega_A \setminus \Gamma_u, \end{cases} \quad (8)$$

$$\mathcal{U} := \{ \mathbf{u}_i \in H_{\Gamma_u}^1(\Omega_A)^N, \mathbf{u}_i = \mathbf{0} \text{ on } \Gamma_u \}, \quad (9)$$

for all indices  $i = 1, 2, \dots, m$ , where  $N$  is the number of spatial dimensions. The inherent strain  $\boldsymbol{\varepsilon}^{inh}$  at the domain  $\Omega_{inh}$  is defined as:

$$\boldsymbol{\varepsilon}^{inh}(\mathbf{x}) = \begin{cases} \boldsymbol{\varepsilon}^{inh} & \text{for } \mathbf{x} \in \Omega_{inh}, \\ \mathbf{0} & \text{otherwise,} \end{cases} \quad (10)$$

where  $\mathbf{x}$  represents a point located in  $\Omega_A$ . The method for identifying the inherent strain components of Eq. 10 is described in the next section.

## 2.2. AM building process model

The AM building process is represented by various activation strategies in finite element modeling [28, 31, 33, 34, 36]. In this study, we use a method in which the inactive domain is activated sequentially from the bottom domain and the inherent strain is applied to each activated domain. To solve the analysis domain  $\Omega$  by the finite element method (FEM), we use an ersatz material approach in which the inactive domain  $\Omega_I$  is occupied by a structural material with a relatively small elastic tensor.

Our AM building process algorithm is as follows.

**Step1.** Inactivate all domains in the analysis domain divided into  $m$  layers.

**Step2.** The domains are activated one by one from the bottom domain, that is, the activated domain is replaced by the original elastic tensor and applied the inherent strain.

**Step3.** The displacement field  $\mathbf{u}_i$  defined in Eqs. 8 and 9 is solved using FEM.

**Step4.** If all domains are activated, the procedure is terminated; otherwise, return to the second step.

The number of layers in the analysis domain is divided into several times more layers than an actual material layer thickness in terms of computational effort. This multi-scale modeling enables the prediction of the part-scale residual stress and distortion. The final residual stress  $\boldsymbol{\sigma}$  and distortion  $\mathbf{u}$  of the part are the sums of the residual stress  $\boldsymbol{\sigma}_i$  and distortion  $\mathbf{u}_i$ , respectively, solved for each active domain  $\Omega_A$ , as follows:

$$\boldsymbol{\sigma} = \sum_{i=1}^m \boldsymbol{\sigma}_i \quad \text{for } \mathbf{x} \in \Omega_A, \quad (11)$$

$$\mathbf{u} = \sum_{i=1}^m \mathbf{u}_i \quad \text{for } \mathbf{x} \in \Omega_A. \quad (12)$$

### 3. Inherent strain identification method

#### 3.1. Experimental procedure

The unknown inherent strain component can be identified based on measurements of a deformation caused by releasing the elastic strain [21, 37]. The elastic strain needs to be released by manufacturing technology that does not change the inherent strain, such as wire electric discharge machines (WEDM). Specimens were fabricated using an LPBF machine (EOSINT M280, EOS GmbH) equipped with a 400 W fiber laser (beam diameter: approximately 0.1 mm). Fig. 2 shows the geometry of the specimen and its dimensions.

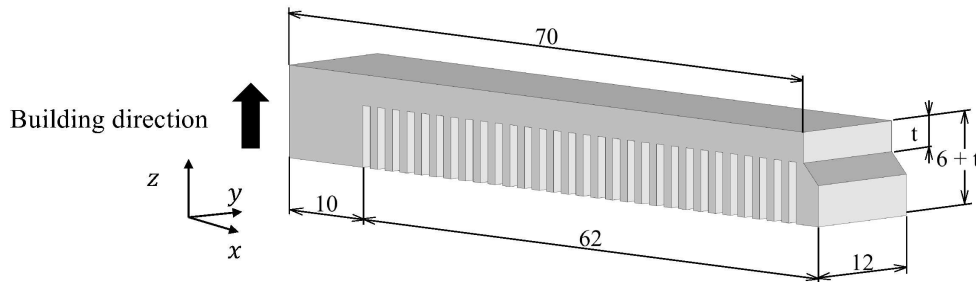


Figure 2: Cantilever specimen with dimensions in mm.

The  $t$  denotes the beam thickness, which is 3 mm. The specimens made of

AlSi10Mg (EOS Aluminum, EOS GmbH) were fabricated on the substrate with an argon atmosphere. The laser scanning parameters used an Original EOS Parameterset adjusted for laser power, scan speed, and scan distance. The laser scanning pattern was rotated  $67^\circ$  layer by layer as shown in Fig. 3 and the constant material layer thickness was 0.03 mm.

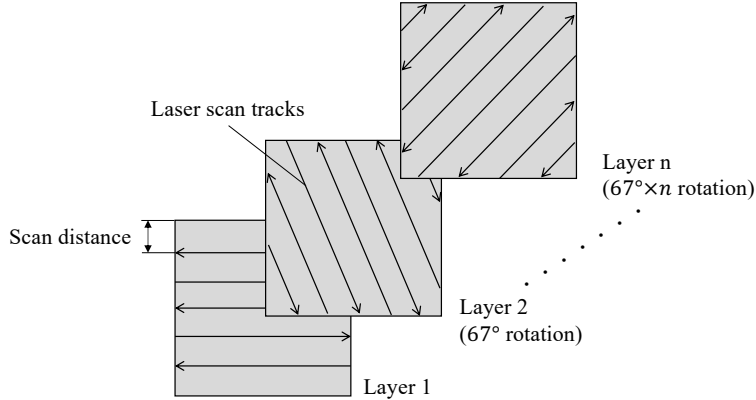


Figure 3: Schematic illustration of laser scanning pattern.

After fabrication, the specimen was partially cut with WEDM at a height of 3 mm from the substrate, leaving the left column attached to the substrate as shown in Fig. 4. By this cutting, the elastic strain is released, leading to large deformation of the specimens. The vertical deformation was calculated from the difference in the top surfaces before and after cutting measured by means of an optical three-dimensional scanner (ATOS Core, GOM GmbH). The inherent strain component is identified from the experimental and numerical results.

### 3.2. Finite element modeling

Figure 5 shows the mesh and analysis conditions for the AM building process and the cutting process. In the AM building process, the displacement of all the bottom surfaces is fixed. The color difference represents each layer to which the inherent strain is applied sequentially. The elasticity problem is solved layer-by-layer according to the AM building process algorithm to determine the elastic strain of the specimen. In the cutting process, only the bottom surface of the left column is fixed, and the elastic strain released by cutting is applied to the part to determine the deformation. The region



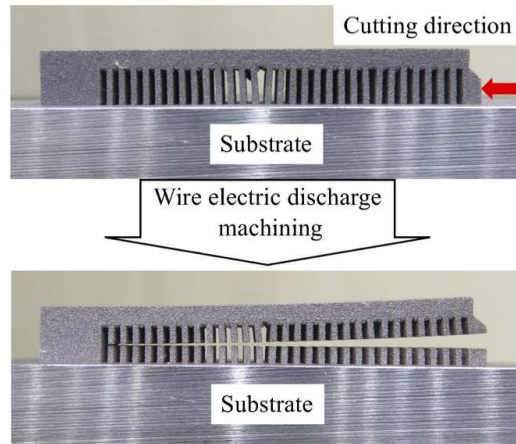


Figure 4: Schematic diagram of cutting the specimens.

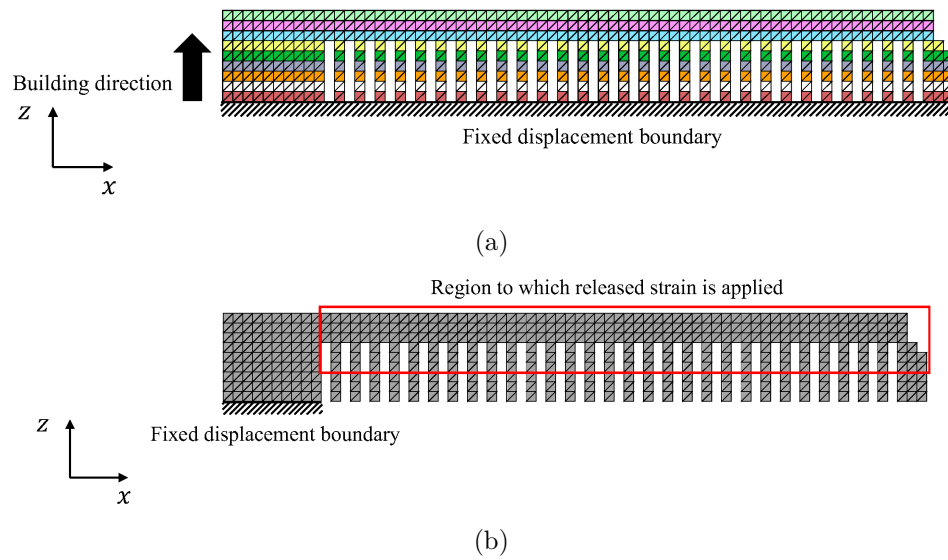


Figure 5: Boundary conditions and mesh model of cantilever beam: (a) AM building process model and (b) cutting model.

of the applied elastic strain is the rectangular area with a red frame (3mm height from the bottom and unfixed area). The layer thickness in the analysis was discretized with an element size of 1 mm, which is about 30 times the actual material layer thickness in the fabrication. The mesh applied to the discretization is a second-order tetrahedral element. In addition, the material properties for the active domains are Young’s modulus = 75 GPa and Poisson’s ratio = 0.34.

### 3.3. Identification procedure

The inherent strain component has been identified under two assumptions. First, fabricated parts shrink isotropically as the laser scan pattern rotates layer by layer. Therefore, the in-plane components is assumed to have the same value [31]. Second, since the layer thickness is sufficiently small compared to the part size, the building direction component can be assumed to be zero [19, 31]. The in-plane inherent strain component were obtained through the minimization of the residual sum of squares of the experimental and numerical vertical deformation results. Figure 6 shows the

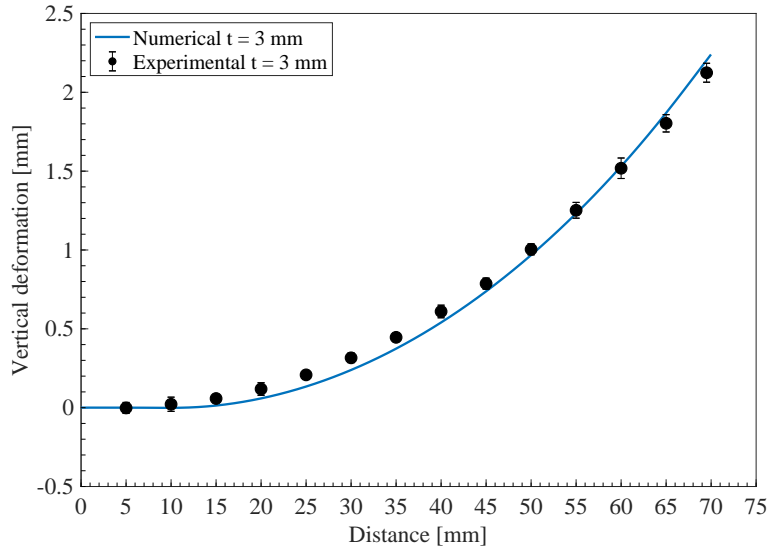


Figure 6: Comparison of experimental and numerical results of vertical deformation after the inherent strain identification procedure.

comparison between numerical and experimental results in terms of vertical deformation of the top surface after minimization. The experimental result

was plotted for the vertical deformation of the top surface at cross-sections measured every 5 mm along the  $x$ -direction. The error bars represent minimum and maximum values in the cross-section. In this case, the in-plane inherent strain component obtained by this procedure is as follows:

$$\boldsymbol{\varepsilon}^{inh} = \begin{Bmatrix} \varepsilon_x \\ \varepsilon_y \\ \varepsilon_z \end{Bmatrix} = \begin{Bmatrix} -0.275 \\ -0.275 \\ 0 \end{Bmatrix}. \quad (13)$$

#### 4. Validation of analytical model

The validity of the identified inherent strain and the proposed analytical model was verified through two types of experiments. First, in order to verify the validity of predicting the distortion, we prepared the cantilever specimen with the beam thickness  $t$  set to 5 mm in Fig. 2 and compared the experimental and numerical results of vertical deformation after cutting the specimen. The cantilever specimen made of AlSi10Mg was fabricated under the same manufacturing conditions as the beam thickness  $t = 3$  mm. After fabrication, the specimen was cut by WEDM and the deformation was measured with the optical three-dimensional scanner. The numerical analysis used the same boundary conditions, the mesh size, material properties, and the inherent strain as the beam thickness  $t = 3$  mm.

Figure 7 shows the comparison between numerical and experimental results in terms of vertical deformation of the top surface. The experimental result was plotted for the vertical deformation of the top surface at cross-sections measured every 5 mm along the  $x$ -direction. The error bars represent minimum and maximum values in the cross-section. The numerical result is consistent with the experimental measurement well. This verification demonstrated that the part-scale distortion induced in the AM building process can be properly predicted.

Next, in order to verify the validity of predicting the residual stress, we compared the experimental and numerical results of the residual stress distribution. A cubic specimen(10mm 10mm 10mm) made of AlSi10Mg was fabricated under the same manufacturing conditions as the cantilever specimen. To measure the residual stress distribution in the building direction, the specimen was successively removed from the top surface by electrolytic polishing and measured by X-ray diffraction stress measurement (-X360, PULSTEC INDUSTRIAL CO., LTD.). The measurement conditions are shown in Table 1. The X-rays were applied to the center of the surface. The specimen

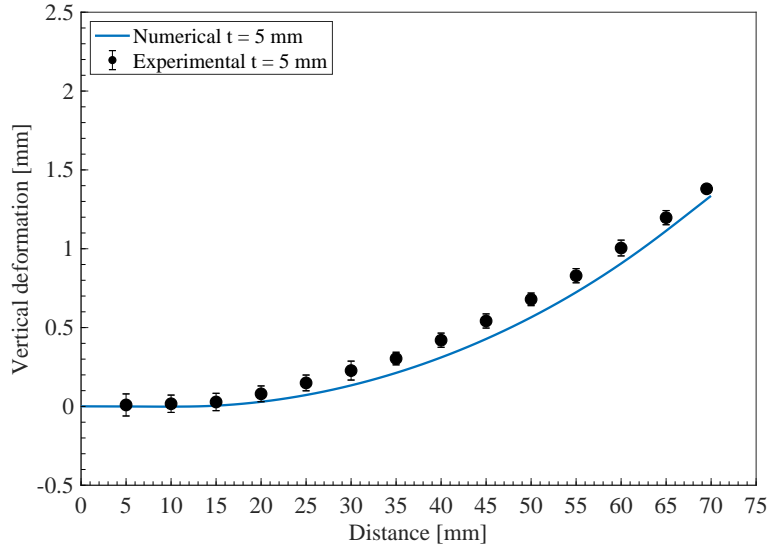


Figure 7: Comparison of experimental and numerical results of vertical deformation after cutting with WEDM.

was removed from the top surface to a depth of 2 mm. Figure 8 shows the

Table 1: Measurement condition.

X-ray tube	Cr-K $\alpha$
Tube voltage / current	30 kV / 1mA
Diffraction plane	Al {2 2 2}
Incident angle	35 deg
Irradiation area	2 mm

boundary condition and mesh in the numerical analysis. The mesh size, material properties, and the inherent strain were set to the same values as in the analysis of the cantilever specimen.

Figure 9 shows the comparison between numerical and experimental results in terms of the residual stress in-depth profile. In both results, it can be seen that the maximum tensile stress was generated on the top surface, and the tensile stress gradually decreased as it got deeper from the surface and turned to compressive stress. This is because when the new layer solidifies and shrinks, it is restrained by the previously solidified layer, causing

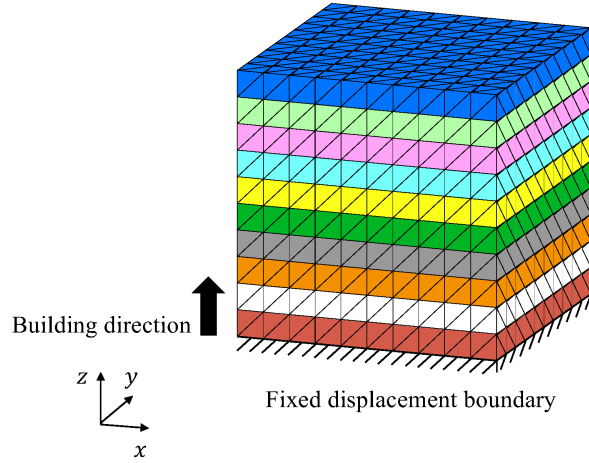


Figure 8: Boundary condition and mesh model of cube.

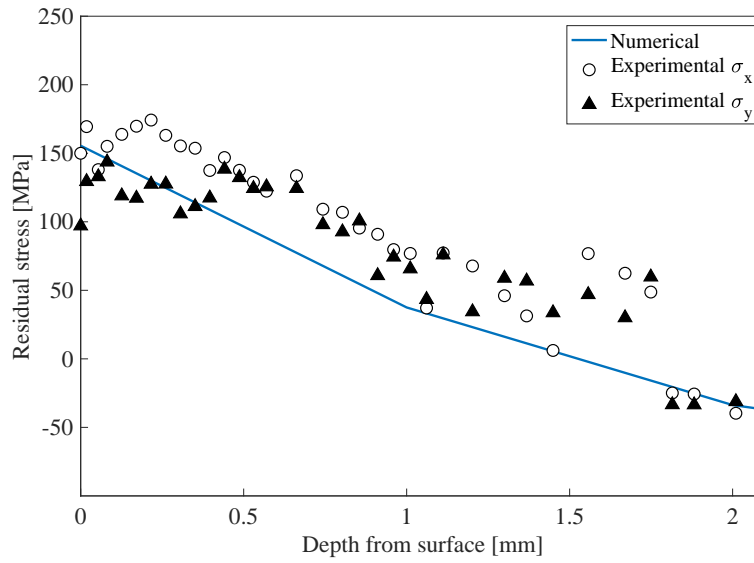


Figure 9: Comparison of experimental and numerical results of the residual stress distribution in-depth profile.

a tensile force on the top surface and a compressive force on the previous layer [14, 18]. This verification demonstrated that the residual stress can be properly predicted by using the inherent strain obtained experimentally. From the above, the validity of the proposed analytical model was confirmed.

## 5. Level set-based topology optimization

The basic idea of topology optimization is to replace the structural optimization problem with the material distribution problem by introducing a fixed design area  $D$  containing the optimal configuration and the characteristic function  $\chi$  as follows:

$$\chi(\mathbf{x}) = \begin{cases} 1 & \text{for } \mathbf{x} \in \Omega, \\ 0 & \text{for } \mathbf{x} \in D \setminus \Omega, \end{cases} \quad (14)$$

where  $\Omega$  is a material domain that denotes the design domain. The above characteristic function makes it possible to represent a configuration with an arbitrary topology. However, it is commonly known that topology optimization problems are ill-posed [38]. Therefore, to convert the well-posed problem, the design domain used some relaxation or regularization techniques. The homogenization design method [1] is a representative approach for relaxing the design domain. On the other hand, level set-based shape and topology optimization methods [39, 40] that regularize the design space have been proposed.

In this study, we use the method of topology optimization that updates the level set function defined as a piecewise constant value function by a time evolution equation. The level set function  $\phi(\mathbf{x})$  that takes real values between -1 and 1 is introduced to represent boundaries  $\partial\Omega$  between the material and void domains, using the iso-surface of  $\phi(\mathbf{x})$  defined as

$$\begin{cases} 0 < \phi(\mathbf{x}) \leq 1 & \text{for } \mathbf{x} \in \Omega \setminus \partial\Omega, \\ \phi(\mathbf{x}) = 0 & \text{for } \mathbf{x} \in \partial\Omega, \\ -1 \leq \phi(\mathbf{x}) < 0 & \text{for } \mathbf{x} \in D \setminus \Omega. \end{cases} \quad (15)$$

The characteristic function  $\chi$  is expressed using the level set function as follows:

$$\tilde{\chi}(\phi) = \begin{cases} 1 & \text{for } \phi(\mathbf{x}) \geq 0, \\ 0 & \text{for } \phi(\mathbf{x}) < 0. \end{cases} \quad (16)$$

Let us consider a structural optimization problem that determines the optimal material distribution using the level set function. That is, the structural optimization problem that finds a level set function that minimizes an objective function is described as follows:

$$\inf_{\phi} F(\tilde{\chi}(\phi), \phi) = \int_D f_d(\mathbf{x})\tilde{\chi}(\phi)d\Omega + \int_{\Gamma} f_b(\mathbf{x})d\Gamma, \quad (17)$$

$$\text{subject to:} \quad \text{governing equation system}, \quad (18)$$

where  $f_d(\mathbf{x})$  and  $f_b(\mathbf{x})$  are the integrands of the objective functional at the fixed design domain and the domain boundaries, respectively. In this study, based on the method of Yamada et al. [40], we replace the problem of finding the optimal distribution of the level set function with a problem that solves the time evolution equation. Assuming the level set function is a function of the introduced fictitious time  $t$ , it is updated by the reaction-diffusion equation as follows:

$$\frac{\partial \phi}{\partial t} = -KF', \quad (19)$$

where  $K$  is a positive parameter and  $F'$  represents the topological derivative [41]. Since the level set function may be discontinuous everywhere in the fixed design domain, the above function is regularized by adding a Laplacian term to the second term on the right side as follows:

$$\frac{\partial \phi}{\partial t} = -K(F' - \tau \nabla^2 \phi), \quad (20)$$

where  $\tau$  is a regularization parameter that affects the degree of diffusivity when updating the level set function, i.e., as  $\tau$  becomes larger, the level set function leads to a smoother distribution [40]. The optimal configuration can be obtained by sequentially updating the level set function using this reaction-diffusion equation.

## 6. Topology optimization considering part distortion in AM

### 6.1. Formulation of optimization problem

We incorporate the proposed AM analytical model into the above optimization framework. The objective functional for reducing the part distortion can be represented by minimizing the following equation:

$$F_{AM} = \left( \int_{\Omega} |\mathbf{u}|^{\beta} d\Omega \right)^{1/\beta}, \quad (21)$$

where  $\beta \geq 2$  is a fixed weighting parameter. Increasing  $\beta$  approaches the minimization of the maximum distortion, and decreasing  $\beta$  approaches the minimization of the average distortion.  $\mathbf{u}$  is the sum of the distortion  $\mathbf{u}_i (i = 1, 2, \dots, m)$  in each active domain  $\Omega_A$  expressed by

$$\mathbf{u} = \sum_{i=1}^m \mathbf{u}_i \quad \text{for } \mathbf{x} \in \Omega_A. \quad (22)$$

In this study, we formulate the minimum mean compliance problem considering the part distortion in AM using the above objective functional. Let us consider the material domain  $\Omega$  that is fixed at boundary  $\Gamma_v$ , with a traction  $\mathbf{t}$  applied at boundary  $\Gamma_t$ . The displacement field is denoted as  $\mathbf{v} \in \mathcal{V}$  in the static equilibrium state. The objective functional of this problem is represented by minimizing the following equation:

$$F_{MC} = \int_{\Gamma_t} \mathbf{t} \cdot \mathbf{v} d\Gamma. \quad (23)$$

Thus, the optimization problem to determine an optimal configuration of the material domain  $\Omega$  that has the minimum mean compliance and the reduction of part distortion under a volume constraint can be formulated as follows:

$$\begin{aligned} \inf_{\tilde{\chi}} \quad & F = (1 - \gamma)F_{MC} + \gamma F_{AM}, \\ \text{subject to: } & G = \int_D \tilde{\chi} d\Omega - V_{\max} \leq 0, \\ & -\operatorname{div}(\mathbb{C}\boldsymbol{\varepsilon}(\mathbf{v})) = 0 \quad \text{in } \Omega, \\ & \mathbf{v} = \mathbf{0} \quad \text{on } \Gamma_v, \\ & -(\mathbb{C}\boldsymbol{\varepsilon}(\mathbf{v})) \cdot \mathbf{n} = \mathbf{0} \quad \text{on } \partial\Omega \setminus \Gamma_t \cup \Gamma_v, \\ & -(\mathbb{C}\boldsymbol{\varepsilon}(\mathbf{v})) \cdot \mathbf{n} = \mathbf{t} \quad \text{on } \Gamma_t, \\ & -\operatorname{div}(\mathbb{C}\boldsymbol{\varepsilon}(\mathbf{u}_i) - \mathbb{C}\boldsymbol{\varepsilon}^{inh}) = 0 \quad \text{in } \Omega_A, \\ & \mathbf{u}_i = \mathbf{0} \quad \text{on } \Gamma_u, \\ & -(\mathbb{C}\boldsymbol{\varepsilon}(\mathbf{u}_i) - \mathbb{C}\boldsymbol{\varepsilon}^{inh}) \cdot \mathbf{n} = \mathbf{0} \quad \text{on } \partial\Omega_A \setminus \Gamma_u, \end{aligned} \quad (24)$$

$$\begin{aligned} \mathcal{V} &:= \{ \mathbf{v} \in H_{\Gamma_u}^1(\Omega)^N, \mathbf{v} = \mathbf{0} \text{ on } \Gamma_v \}, \\ \mathcal{U} &:= \{ \mathbf{u}_i \in H_{\Gamma_v}^1(\Omega_A)^N, \mathbf{u}_i = \mathbf{0} \text{ on } \Gamma_u \}, \end{aligned} \quad (25)$$



for all indices  $i = 1, 2, \dots, m$ , where  $0 \leq \gamma \leq 1$  is a weighting coefficient and  $N$  is the number of spatial dimensions. In the above formulation,  $G$  represents the volume constraint and  $V_{max}$  is the upper limit of the material volume in  $D$ .

## 6.2. Sensitivity analysis

To derive the topological derivative of the above optimization problem, we use the adjoint variable method. First, the minimum mean compliance problem is known to be a self-adjoint problem. Therefore, the adjoint variable corresponds to the displacement field  $\mathbf{v}$ , and the topological derivative of Eq. 23 is given by [42, 43]

$$F'_{MC} = -\boldsymbol{\varepsilon}(\mathbf{v}) : \mathbb{A} : \boldsymbol{\varepsilon}(\mathbf{v}). \quad (26)$$

For a plane stress problem, the above constant fourth-order tensor  $\mathbb{A}$  is given by

$$\mathbb{A}_{ijkl} = \frac{1}{(1 + \nu)^2} \left\{ \frac{-(1 - 6\nu + \nu^2) E}{(1 - \nu)^2} \delta_{ij} \delta_{kl} + 2E (\delta_{ik} \delta_{jl} + \delta_{il} \delta_{jk}) \right\}. \quad (27)$$

Next, let us consider an adjoint state  $\tilde{\mathbf{u}}_i \in \mathcal{U}$  regarding the displacement field  $\mathbf{u}_i$  of the part distortion in AM. Associated with the objective functional Eq. 21 we introduce the following adjoint system:

$$\begin{cases} -\text{div}(\mathbb{C}\boldsymbol{\varepsilon}(\tilde{\mathbf{u}}_i)) = - \left( \int_{\Omega} |\mathbf{u}|^{\beta} d\Omega \right)^{1/\beta-1} |\mathbf{u}|^{\beta-1} & \text{in } \Omega_A, \\ \tilde{\mathbf{u}}_i = \mathbf{0} & \text{on } \Gamma_u, \\ -(\mathbb{C}\boldsymbol{\varepsilon}(\tilde{\mathbf{u}}_i)) \cdot \mathbf{n} = \mathbf{0} & \text{on } \partial\Omega_A \setminus \Gamma_u, \end{cases} \quad (28)$$

for all indices  $i = 1, 2, \dots, m$ , and the topological derivative of Eq. 21 is as follows [44]:

$$F'_{AM} = \sum_{i=1}^m \left( -\boldsymbol{\varepsilon}(\mathbf{u}_i) : \mathbb{A} : \boldsymbol{\varepsilon}(\tilde{\mathbf{u}}_i) + \boldsymbol{\varepsilon}^{inh} : \mathbb{A} : \boldsymbol{\varepsilon}(\tilde{\mathbf{u}}_i) \right). \quad (29)$$

## 7. Numerical implementation

### 7.1. Optimization algorithm

The optimization algorithm is as follows.

- Step1.** The initial level set function is set.
- Step2.** The displacement fields  $\mathbf{v}$  and  $\mathbf{u}_i$  defined in Eqs. 24 and 25 are solved using FEM.
- Step3.** The objective functional  $F$  consisting of Eqs. 21 and 23 is calculated.
- Step4.** If the objective functional is converged, the optimization procedure is terminated; otherwise, the adjoint field  $\tilde{\mathbf{u}}_i$  defined in Eq. 28 is solved using FEM, and the topological derivatives with respect to the objective functional are calculated using Eqs. 26 and 29.
- Step5.** The level set function is updated using the time evolution equation defined in Eq. 20 and the optimization procedure then returns to the second step.

### 7.2. Numerical scheme for governing equation

The finite elements are generated during the iterative optimization procedure. From the perspective of computational effort, we use the ersatz material approach [39]. Assume that the void domain is a structural material with a relatively small elastic tensor and that the boundary of the material and void domain has a smoothly distributed material property; that is, we use the extended elastic tensor  $\tilde{\mathbb{C}}$  to solve the governing equations in the fixed design domain  $D$ , as follows:

$$\tilde{\mathbb{C}}(\phi; w) = \{(1 - d)H(\phi; w) + d\} \mathbb{C}, \quad (30)$$

where the  $H(\phi; w)$  is defined as:

$$H(\phi; w) := \begin{cases} 1 & \text{for } \phi > w, \\ \frac{1}{2} + \frac{\phi}{w} \left( \frac{15}{16} - \frac{\phi^2}{w^2} \left( \frac{5}{8} - \frac{3}{16} \frac{\phi^2}{w^2} \right) \right) & \text{for } -w \leq \phi \leq w, \\ 0 & \text{for } \phi < -w, \end{cases} \quad (31)$$

where  $w$  represents the width of the transition and  $d$  represents the ratio of the Young's modulus for the two materials, one structural and the other void.

### 7.3. Normalization for topological derivative scaling

The scale of topological derivative  $F'_{MC}$  and  $F'_{AM}$  is significantly affected by the fixed design domain scale and boundary condition settings. Therefore, we use a normalized topological derivative  $\tilde{F}'$ , as follows:

$$\tilde{F}' = (1 - \gamma) \frac{F'_{MC} \int_D d\Omega}{\int_D |F'_{MC}| d\Omega} + \gamma \frac{F'_{AM} \int_D d\Omega}{\int_D |F'_{AM}| d\Omega}. \quad (32)$$

## 8. Numerical examples

In this section, numerical examples are presented to demonstrate the utility and validity of proposed optimization methodology for two-dimensional minimum compliance problems considering the part distortion in AM. The fixed design domain and boundary conditions of the two models are shown in Fig. 10 and Fig. 11, respectively. The fixed design domain in Fig. 10(b) and Fig. 11(b) is divided into  $m = 56$  and  $m = 50$  layers, respectively, with a layer thickness of 1 in the building direction. The elastic material has Young's modulus = 75 GPa and Poisson's ratio = 0.34. The applied traction  $t$  was set to 100 and the inherent strain component was set to the value in Eq. 13. The upper limit of the allowable volume was set to 50% of the volume of the fixed design domain. The regularization parameter  $\tau$  was set to  $1 \times 10^{-4}$  for the cantilever model and  $1 \times 10^{-3}$  for the MBB beam model. The weighting parameter  $\beta$  in Eq. 24 was set to 6. The parameters  $w$  and  $d$  in Eq. 31 were set to 0.5 and  $1 \times 10^{-3}$ , respectively. We examined the dependency of the optimal configurations with respect to different settings of parameter  $\gamma$ . Figures 12 and 13 show various obtained optimal configurations for each model. Figure 14 shows a plot of each objective functional corresponding to the varying weighting coefficient. For  $\gamma = 0$  denotes that the objective functional is only a compliance minimization problem. As shown in Fig. 14, when the weighting coefficient  $\gamma$  is set larger, the objective functional that represents the part distortion in AM decreases, and the compliance increases. Therefore, by adjusting  $\gamma$ , compliance and part distortion can be controlled. That is, the part with the desired performance can be manufactured with high dimensional accuracy by AM. If the target distortion  $\mathbf{u}_0$  is introduced and replaced with  $\mathbf{u} = \mathbf{u} - \mathbf{u}_0$  in Eq. 21, it can be manufactured with arbitrary dimensional accuracy. Figure 15 shows a convergence history of the objective functional and volume constraint for the

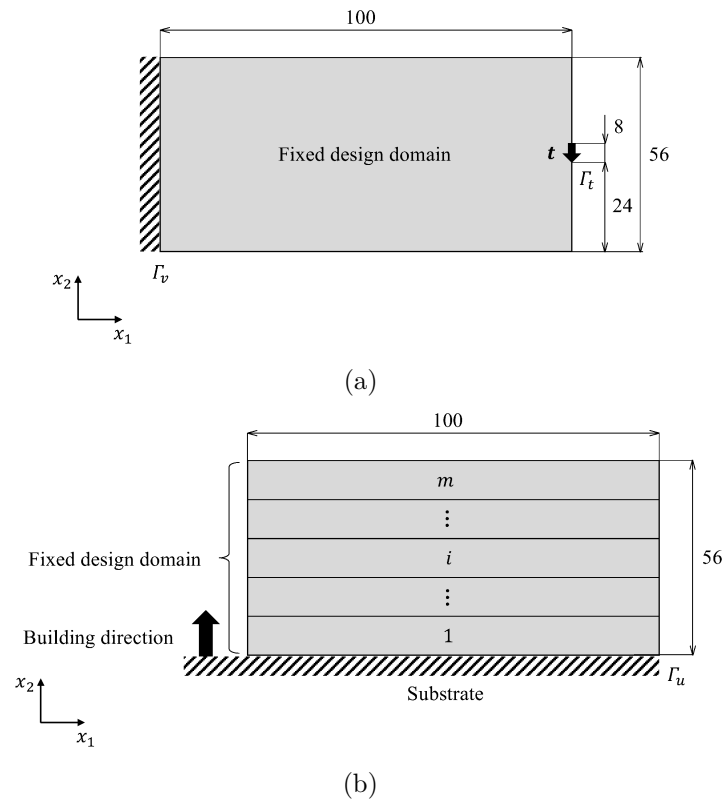


Figure 10: Fixed design domain and boundary conditions for cantilever model: (a) minimum mean compliance problem and (b) mechanics problem of AM.

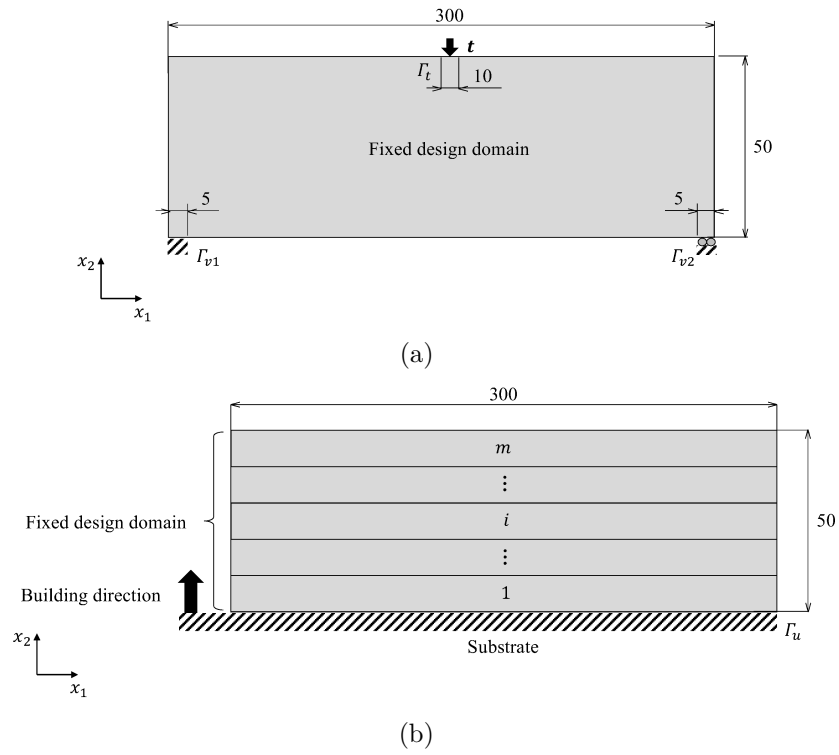


Figure 11: Fixed design domain and boundary conditions for MBB beam model: (a) minimum mean compliance problem and (b) mechanics problem of AM.

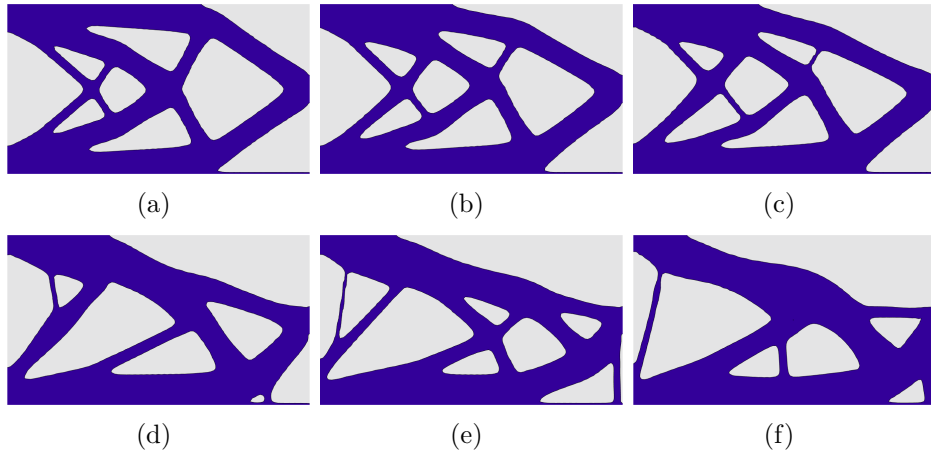


Figure 12: Optimal configurations for cantilever model: (a) $\gamma = 0$ ; (b) $\gamma = 0.04$ ; (c) $\gamma = 0.06$ ; (d) $\gamma = 0.08$ ; (e) $\gamma = 0.10$ ; (f) $\gamma = 0.15$ .

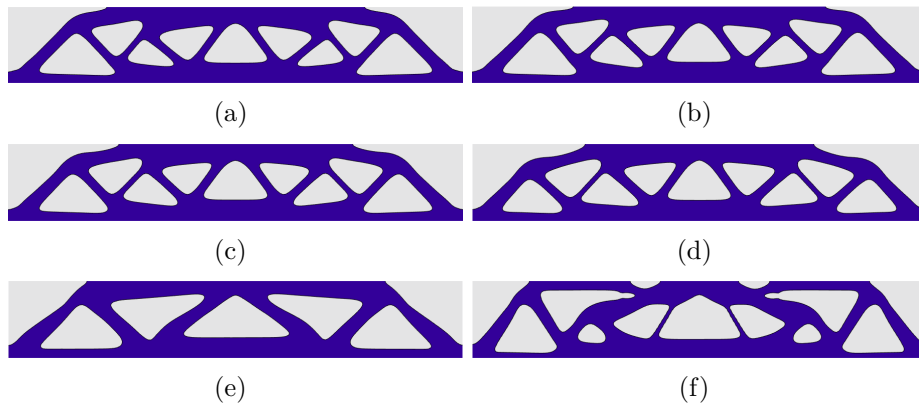


Figure 13: Optimal configurations for MBB beam model: (a) $\gamma = 0$ ; (b) $\gamma = 0.04$ ; (c) $\gamma = 0.06$ ; (d) $\gamma = 0.10$ ; (e) $\gamma = 0.15$ ; (f) $\gamma = 0.20$ .

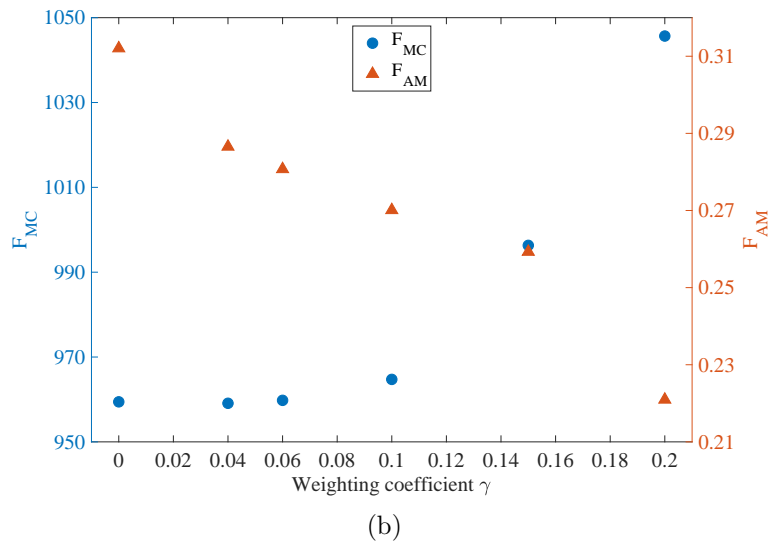
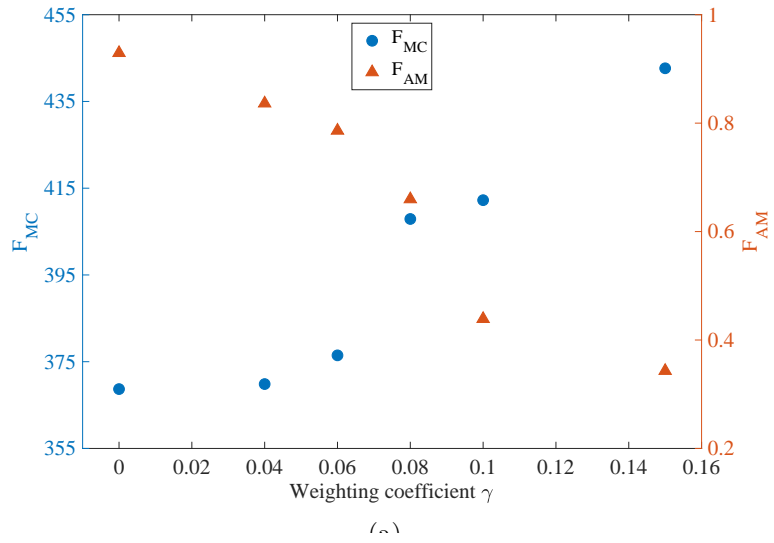


Figure 14: Objective functional with different weighting coefficient  $\gamma$ : (a)cantilever model; (b)MBB beam model.

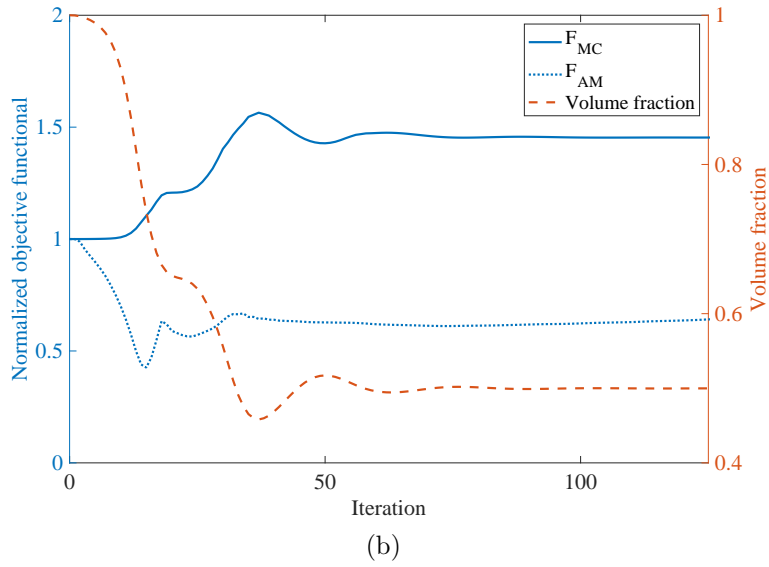
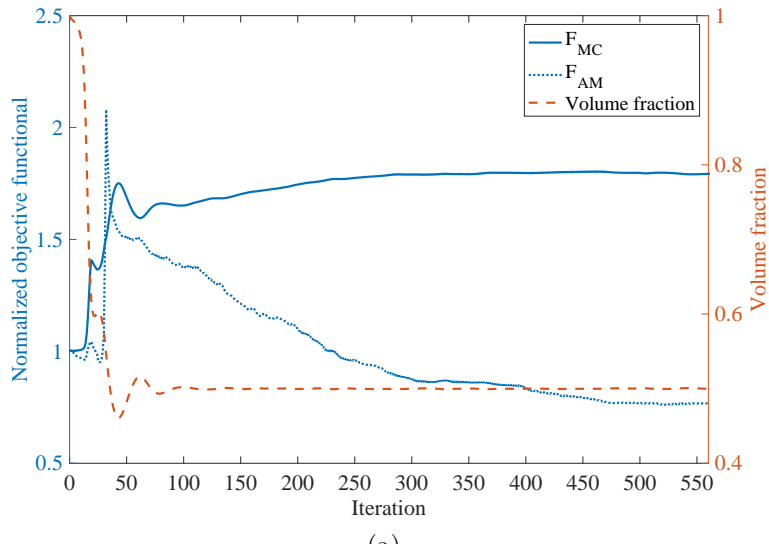
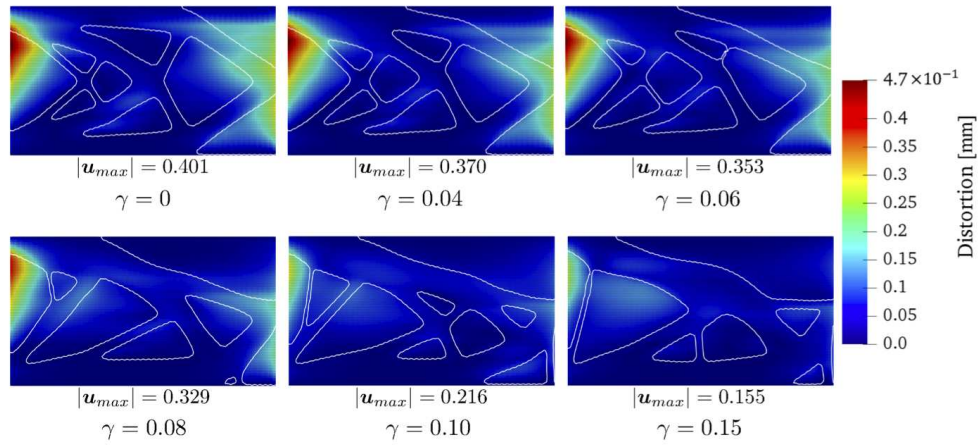
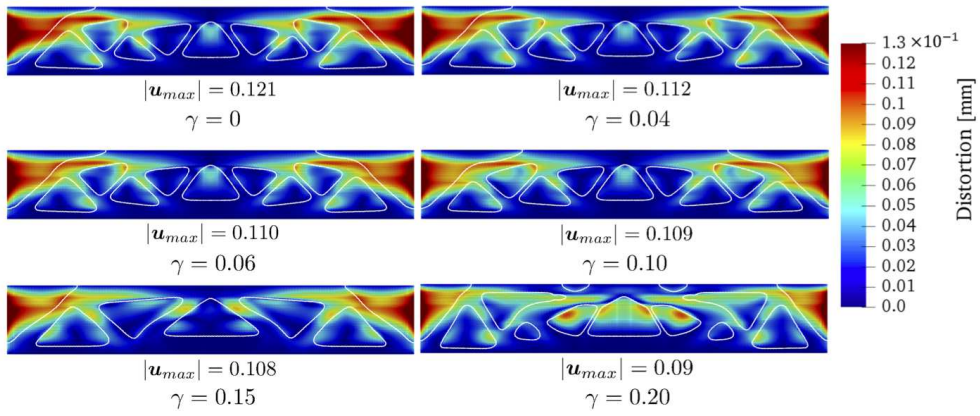


Figure 15: Convergence history of objective functional and volume constraint for the case of  $\gamma = 0.1$ : (a)cantilever model; (b)MBB beam model.





(a)



(b)

Figure 16: Numerical results of part distortion induced by AM process: (a)cantilever model; (b)MBB beam model.

case of  $\gamma = 0.1$  for each model. As the number of iterations increases, the objective functional for the part distortion in AM decreases and the compliance is maintained while satisfying the volume constraint. Figure 16 shows the numerical results of the part distortion induced by AM for the final shape. As  $\gamma$  increases, the maximum displacement decreases, and the displacement distribution in the material domain becomes uniform. This proves that the proposed methodology is efficient in considering the part distortion in AM.

## 9. Conclusion

In this paper, we proposed a topology optimization method that considers the part distortion in AM, using a computationally inexpensive analytical model. We achieved the following:

1. To predict the part-scale residual stress and distortion induced in the AM building process, the AM analytical model based on the inherent strain method and the identification method of the inherent strain component was proposed. The experimentally identified in-plane inherent strain component and building process algorithm in the analytical model have been demonstrated to properly predict the part-scale residual stress and distortion without using coupled or nonlinear analysis.
2. An objective functional for reducing the part distortion in AM was proposed, and a minimum mean compliance problem considering the part distortion in AM was formulated. In the numerical implementation, an optimization algorithm was constructed and the non-dimensional sensitivity was used to enable simple adjustment of a weighting coefficient  $\gamma$ .
3. In the minimum mean compliance problem, the proposed method provided an optimal configuration in which the compliance and the part distortion in AM can be controlled by adjusting  $\gamma$  appropriately.

## 10. Acknowledgments

The authors are grateful to S. Nishiwaki and K. Furuta for useful discussions. We also thank K. Murata for technical assistance with X-ray stress measurement experiments. This work was supported by JSPS Grant for Scientific Research(B) JP19H02049.

## References

- [1] M. P. Bendsoe, N. Kikuchi, Generating optimal topologies in structural design using a homogenization method, *Computer Methods in Applied Mechanics and Engineering* 71 (2) (1988) 197–224.
- [2] M. P. Bendsøe, Optimal shape design as a material distribution problem, *Structural Optimization* 1 (4) (1989) 193–202.
- [3] G. Allaire, F. Jouve, G. Michailidis, Thickness control in structural optimization via a level set method, *Structural and Multidisciplinary Optimization* 53 (6) (2016) 1349–1382.
- [4] T. Yamada, Thickness constraints for topology optimization using the fictitious physical model, in: *International Conference on Engineering Optimization*, Springer, 2018, pp. 483–490.
- [5] Q. Xia, T. Shi, M. Y. Wang, S. Liu, A level set based method for the optimization of cast part, *Structural and Multidisciplinary Optimization* 41 (5) (2010) 735–747.
- [6] G. Allaire, F. Jouve, G. Michailidis, Molding direction constraints in structural optimization via a level-set method, in: *Variational Analysis and Aerospace Engineering*, Springer, 2016, pp. 1–39.
- [7] Y. Sato, T. Yamada, K. Izui, S. Nishiwaki, Manufacturability evaluation for molded parts using fictitious physical models, and its application in topology optimization, *The International Journal of Advanced Manufacturing Technology* 92 (1-4) (2017) 1391–1409.
- [8] M. Leary, L. Merli, F. Torti, M. Mazur, M. Brandt, Optimal topology for additive manufacture: A method for enabling additive manufacture of support-free optimal structures, *Materials & Design* 63 (2014) 678–690.
- [9] M. Langelaar, Topology optimization of 3d self-supporting structures for additive manufacturing, *Additive Manufacturing* 12 (2016) 60–70.
- [10] A. T. Gaynor, J. K. Guest, Topology optimization considering overhang constraints: Eliminating sacrificial support material in additive manufacturing through design, *Structural and Multidisciplinary Optimization* 54 (5) (2016) 1157–1172.

- [11] G. Allaire, C. Dapogny, R. Estevez, A. Faure, G. Michailidis, Structural optimization under overhang constraints imposed by additive manufacturing technologies, *Journal of Computational Physics* 351 (2017) 295–328.
- [12] Y. Wang, J. Gao, Z. Kang, Level set-based topology optimization with overhang constraint: towards support-free additive manufacturing, *Computer Methods in Applied Mechanics and Engineering* 339 (2018) 591–614.
- [13] J.-P. Kruth, L. Froyen, J. Van Vaerenbergh, P. Mercelis, M. Rombouts, B. Lauwers, Selective laser melting of iron-based powder, *Journal of Materials Processing Technology* 149 (1-3) (2004) 616–622.
- [14] P. Mercelis, J.-P. Kruth, Residual stresses in selective laser sintering and selective laser melting, *Rapid Prototyping Journal* (2006).
- [15] L. Van Belle, G. Vansteenkiste, J. C. Boyer, Investigation of residual stresses induced during the selective laser melting process, in: *Key Engineering Materials*, Vol. 554, Trans Tech Publ, 2013, pp. 1828–1834.
- [16] A. S. Wu, D. W. Brown, M. Kumar, G. F. Gallegos, W. E. King, An experimental investigation into additive manufacturing-induced residual stresses in 316l stainless steel, *Metallurgical and Materials Transactions A* 45 (13) (2014) 6260–6270.
- [17] O. Fergani, F. Berto, T. Welo, S. Liang, Analytical modelling of residual stress in additive manufacturing, *Fatigue & Fracture of Engineering Materials & Structures* 40 (6) (2017) 971–978.
- [18] C. Li, Z. Liu, X. Fang, Y. Guo, Residual stress in metal additive manufacturing, *Procedia Cirp* 71 (2018) 348–353.
- [19] M. Bugatti, Q. Semeraro, Limitations of the inherent strain method in simulating powder bed fusion processes, *Additive Manufacturing* 23 (2018) 329–346.
- [20] Y. Ueda, T. Yamakawa, Analysis of thermal elastic-plastic stress and strain during welding by finite element method, *Japan Welding Society Transactions* 2 (2) (1971).

- [21] Y. Ueda, K. Fukuda, K. Nakacho, S. Endo, A new measuring method of residual stresses with the aid of finite element method and reliability of estimated values, *Journal of the Society of Naval Architects of Japan* 1975 (138) (1975) 499–507.
- [22] H. Murakawa, Y. Luo, Y. Ueda, Prediction of welding deformation and residual stress by elastic fem based on inherent strain, *Journal of the society of Naval Architects of Japan* 1996 (180) (1996) 739–751.
- [23] L. Papadakis, A. Loizou, J. Risse, J. Schrage, Numerical computation of component shape distortion manufactured by selective laser melting, *Procedia Cirp* 18 (2014) 90–95.
- [24] N. Hodge, R. Ferencz, J. Solberg, Implementation of a thermomechanical model for the simulation of selective laser melting, *Computational Mechanics* 54 (1) (2014) 33–51.
- [25] C. Li, C. Fu, Y. Guo, F. Fang, A multiscale modeling approach for fast prediction of part distortion in selective laser melting, *Journal of Materials Processing Technology* 229 (2016) 703–712.
- [26] T. Mukherjee, W. Zhang, T. DebRoy, An improved prediction of residual stresses and distortion in additive manufacturing, *Computational Materials Science* 126 (2017) 360–372.
- [27] E. R. Denlinger, M. Gouge, J. Irwin, P. Michaleris, Thermomechanical model development and in situ experimental validation of the laser powder-bed fusion process, *Additive Manufacturing* 16 (2017) 73–80.
- [28] M. Chiumenti, E. Neiva, E. Salsi, M. Cervera, S. Badia, J. Moya, Z. Chen, C. Lee, C. Davies, Numerical modelling and experimental validation in selective laser melting, *Additive Manufacturing* 18 (2017) 171–185.
- [29] C. Li, J. Liu, X. Fang, Y. Guo, Efficient predictive model of part distortion and residual stress in selective laser melting, *Additive Manufacturing* 17 (2017) 157–168.
- [30] N. Keller, V. Ploshikhin, New method for fast predictions of residual stress and distortion of am parts, in: *Solid Freeform Fabrication Symposium*, Vol. 25, 2014.

- [31] I. Setien, M. Chiumenti, S. van der Veen, M. San Sebastian, F. Garciaandía, A. Echeverría, Empirical methodology to determine inherent strains in additive manufacturing, *Computers & Mathematics with Applications* 78 (7) (2019) 2282–2295.
- [32] Q. Chen, X. Liang, D. Hayduke, J. Liu, L. Cheng, J. Oskin, R. Whitmore, A. C. To, An inherent strain based multiscale modeling framework for simulating part-scale residual deformation for direct metal laser sintering, *Additive Manufacturing* 28 (2019) 406–418.
- [33] R. A. Wildman, A. T. Gaynor, Topology optimization for reducing additive manufacturing processing distortions, Tech. rep., Weapons and Materials Research Directorate, US Army Research Laboratory (2017).
- [34] G. Allaire, L. Jakabčín, Taking into account thermal residual stresses in topology optimization of structures built by additive manufacturing, *Mathematical Models and Methods in Applied Sciences* 28 (12) (2018) 2313–2366.
- [35] F. Hecht, New development in freefem++, *J. Numer. Math.* 20 (3-4) (2012) 251–265.  
URL <https://freefem.org/>
- [36] P. Foteinopoulos, A. Papacharalampopoulos, P. Stavropoulos, On thermal modeling of additive manufacturing processes, *CIRP Journal of Manufacturing Science and Technology* 20 (2018) 66–83.
- [37] Y. Ueda, K. Fukuda, M. Tanigawa, New measuring method of three dimensional residual stresses based on theory of inherent strain (welding mechanics, strength & design), *Transactions of JWRI* 8 (2) (1979) 249–256.
- [38] G. Allaire, Shape optimization by the homogenization method, Vol. 146, Springer-Verlag, 2002.
- [39] G. Allaire, F. Jouve, A.-M. Toader, Structural optimization using sensitivity analysis and a level-set method, *Journal of Computational Physics* 194 (1) (2004) 363–393.

- [40] T. Yamada, K. Izui, S. Nishiwaki, A. Takezawa, A topology optimization method based on the level set method incorporating a fictitious interface energy, *Computer Methods in Applied Mechanics and Engineering* 199 (45-48) (2010) 2876–2891.
- [41] S. Amstutz, H. Andrä, A new algorithm for topology optimization using a level-set method, *Journal of Computational Physics* 216 (2) (2006) 573–588.
- [42] S. Garreau, P. Guillaume, M. Masmoudi, The topological asymptotic for pde systems: the elasticity case, *SIAM Journal on Control and Optimization* 39 (6) (2001) 1756–1778.
- [43] R. Feijoo, A. Novotny, E. Taroco, C. Padra, The topological-shape sensitivity method in two-dimensional linear elasticity topology design, *Applications of Computational Mechanics in Structures and Fluids* (2005).
- [44] S. M. Giusti, Z. Mróz, A. Novotny, J. Sokołowski, Topology design of thermomechanical actuators, *Structural and Multidisciplinary Optimization* 55 (5) (2017) 1575–1587.